

# Muscle Bioenergetics of Speeding Fish: In Vivo MRS Studies in a 4.7 T Magnetic Resonance Scanner with an Integrated Swim Tunnel

CHRISTIAN BOCK,<sup>1</sup> GLENN J. LURMAN,<sup>1,2</sup> ROLF-M. WITTIG,<sup>1,2</sup> DALE M. WEBBER,<sup>2</sup> HANS-O. PÖRTNER<sup>1,2</sup>

<sup>1</sup>Department of Marine Animal Physiology, Division of Biosciences, Alfred Wegener Institute for Polar and Marine Research, Am Handelshafen 12, 27570 Bremerhaven, Germany

<sup>2</sup>Vemco, A Division of Amirix Systems, 77 Chain Lake Drive, Halifax, Nova Scotia, Canada B3S 1E1

**ABSTRACT:** Energetic studies on exercising animals are usually limited to oxygen consumption measurements in respirometers followed by invasive tissue sampling and analysis of metabolites. Noninvasive studies of exercising animals like through the use of <sup>31</sup>P NMR are typically restricted to “stop and go” measurements. Furthermore, magnetic resonance studies of marine animals are hampered by sea water, a highly electric conductive and dielectric medium, resulting in heavy loading and strong RF loss. In this work, we present a set-up for online determination of muscle bioenergetics in swimming marine fish, Atlantic cod (*Gadus morhua*), using in vivo <sup>31</sup>P NMR spectroscopy, which overcome these limitations. Special hardware and RF coils were developed for this purpose. A birdcage resonator adapted to high loadings was used for signal excitation. An insulated inductive coil (2 cm diameter) was fixed onto the surface of the fish tail and placed opposite a watertight, passively decoupled 9 × 6 cm<sup>2</sup> elliptic and curved surface coil for signal recordings. This arrangement led to enhanced penetration of the RF signal and an almost 10-fold increase in S/N ratio compared to the exclusive use of the elliptic surface coil. Monitoring of tail beat allowed to set trigger values resulted in an improved quality of in vivo <sup>31</sup>P NMR spectra of swimming fish. We report the first successful MRS experiments recording simultaneously tissue energetic and acid–base parameters on swimming cod depending on tail beat frequency and amplitude to determine critical swimming speeds. © 2007 Wiley Periodicals, Inc. Concepts Magn Reson Part B (Magn Reson Engineering) 00B: 000–000, 2007

**KEY WORDS:** <sup>31</sup>P NMR; MRS; MRI; RF coils; trigger; gating; swim tunnel; conductivity; exercise; Atlantic cod; *Gadus morhua*; energy metabolism

Received 13 July 2007; revised 22 October 2007; accepted 23 October 2007

Correspondence to: Dr. Christian Bock; E-mail: Christian.Bock@awi.de

Part of this work was presented at the ISMRM 2002 in Honolulu, Hawaii, USA

Concepts in Magnetic Resonance Part B (Magnetic Resonance Engineering), Vol. 00B(0) 000–000 (2007)

Published online in Wiley InterScience (www.interscience.wiley.com). DOI 10.1002/cmr.b.20105

© 2007 Wiley Periodicals, Inc.

## INTRODUCTION

Muscle physiology and energy metabolism under basal and exercise conditions have received significant attention, both for an understanding of the factors enabling and limiting exercise and, more recently, for an understanding of the role of temperature adaptation and acclimation shaping exercise performance in marine animals from various climate regimes (1–3). The function and organization of muscle tissue from ectothermic animals living at low or polar tempera-

tures is especially interesting, and studies revealed unique features of adaptation for living and swimming in cold waters at all organismic levels. Briefly, cold adaptation characteristics include a specialized muscle anatomy with an increased mitochondrial proliferation (for a review, see 4), antifreeze proteins (for a review, see 5), modified membrane structures and functions using unsaturated phospholipids (e.g., 6), and specialized modes of energy metabolism including increased lipid  $\beta$ -oxidation rather than glycolysis (3). An increase of lipid content will facilitate oxygen diffusion in muscle (7). Some of these features are also expressed in cold acclimated temperate fish-like crucian carp that displays increased mitochondrial densities in muscle tissue of up to 45% (8).

Little is known about the functional consequences of these mechanisms for example during exercise (9; for reviews, see 3, 4). An understanding of these special adaptations is becoming even more important in the framework of climate change, questioning how animals specialized on limited climate and temperature regimes can cope with rising temperatures? A model explaining the oxygen limitation of thermal tolerance has recently been developed and tested in an ecological context with the goal to explain these phenomena (1–3, 10). These analyses revealed a key role for the thermal sensitivity of aerobic scope and the mechanisms shaping the thermal window of aerobic scope. In the context of exercise physiology, aerobic scope is defined as the difference between basal and maximal or active metabolism (11, 12). Classical oxygen consumption measurements of aerobic scope are often hampered by the experimental set-up so that reliable results are difficult to obtain within a typical experimental time frame (12). Any invasive studies for measurements of additional parameters like circulatory performance, blood-gas transport, or muscle perfusion in marine animals will complicate the situation further due to lower performance and increased recovery rates after surgery. For example, rainbow trout needed more or less 48 h to reestablish control values after surgery and implantation of oxygen probes into gill arteries (13). Noninvasive studies like  $^{31}\text{P}$  NMR analyses on exercising animals have previously been restricted to “stop and go” measurements (14). To overcome this dilemma, we developed a minimally invasive set-up that measured several parameters correlated with aerobic scope during exercise of free-swimming fish.

The aim of this work was to develop an experimental set-up for the online determination of aerobic scope, oxygen consumption, and swimming performance, combined with studies of muscle energy metab-

olism and acid–base regulation by in vivo  $^{31}\text{P}$  NMR spectroscopy of fish. For this purpose, a Brett type swim tunnel respirometer was integrated into a 4.7 T MRI scanner (Bruker Biospec, Ettlingen, Germany).

Magnetic resonance (MR) measurements in electrically conductive, dielectric media are complicated mainly by inductive losses. These losses originate from eddy currents induced within the sample by the oscillating field  $B_1$ . The electric conductivity decreases the signal-to-noise ratio ( $S/N$ ); the loading in a coil rises. Also, pulse length or power to produce a given pulse angle increases, whereas the irradiation of radio frequencies (RFs) is attenuated due to the skin effect. These strong effects might even be intensified when an electrically conductive medium like sea water is flowing through an NMR probe. Principally, the induction of eddy currents must be avoided. In the case of surrounding sea water, this is usually only possible if the sensitive volume inside a probe is divided into specific parts by use of electrical insulators (15). However, this is not applicable to in vivo NMR studies, due to the limited space available inside an NMR probe, especially in the case of freely moving animals. Our approach was therefore mainly to adapt and optimize the RF-hardware with respect to the specific requirements for swimming marine fish in a horizontal MR scanner.

## MATERIALS AND METHODS

### Animals

Two groups of Atlantic cod (*Gadus morhua*) from the North East Arctic and the North Sea, with a body length between 35 and 52 cm and 0.5–1.1 kg body weight were used for a comparative NMR study (data and results will be presented in an accompanying publication, 16). Briefly, North Sea cod were caught in the German Bight by bottom trawls or bow nets on the White Bank near Helgoland. They were transported by RV “Heinke” or RC “Uthörn” to Bremerhaven and kept in natural sea water of the aquarium system of the Alfred Wegener Institute at temperatures around 10°C. Animals were fed frozen mussels, *Mytilus edulis*, or frozen shrimps, *Crangon crangon* twice a week. Feeding was stopped at least 1 week prior to experimentation. Cultured North Eastern Arctic cod were a generous gift from Dr. M. Delghandi at the IMR in Tromsø and transported to the AWI by air. Animals from both groups were kept in aquarium tanks with a volume of 1 m<sup>3</sup> under identical conditions (see accompanying paper for more details, 16).

## Surgery

All animals were anesthetized with 0.08 g/l MS222 and body weights and lengths were measured. During surgery gills were irrigated continuously with aerated sea water containing 0.04 g/l MS222. An inductive coil (2 cm inner diameter, tuned to a fixed frequency of 81 MHz, covered and sealed in plastic, with a final size of a  $4.5 \times 4.5 \text{ cm}^2$ ) was sewn with two sutures to the skin just prior to the tail on one side of the fish. During an initial set of experiments, the caudal fin was punctured and fitted with a differential pressure transducer, which was fixed with suture onto the skin for online monitoring of tail beat pressures and frequency (17–19). The complete surgical procedure lasted no longer than 20 min. All animals survived the experimental procedure.

## Swim Tunnel Set-Up

A “Brett-type” swim tunnel respirometer was constructed and fed through the 40 cm inner diameter of a Bruker Biospec 47/40 DBX system, operated at 4.7 T (Fig. 1). Briefly, a 2 m Perspex pipe (wall thickness 1 cm, inner diameter 17.5 cm) was fed through the MR scanner. Special custom-made adapters with an outside rubber seal and plastic clip collars provided fitting to standard PVC tubes of 10 cm inner diameter. In all other cases, union nuts with compression rings were used as connectors. An animal handling chamber was placed directly in front of the magnet for the preparation of the animal and the MR set-up. Both ends of the circular tube ended in a round Perspex reservoir with a maximum volume of around 450 l. The reservoir was connected to a separate filter and cooling system consisting of a heat exchanger (Calorplast Wärmetechnik GmbH, Germany) and a cooler with a maximum cooling rate of 12.5 kW. A protein skimmer combined with a trickle filter was connected to the sea water reservoir. An additional cooling coil was inserted into the tube system and connected to a cryostat (Lauda, Germany) to provide constant temperatures between 0 and 20°C during closed system operations. Temperature stability was around  $\pm 0.5^\circ\text{C}$  in both open and closed system operation. A circulation pump (Jesco Dosiertechnik, Germany) with a maximum output of 30 m<sup>3</sup>/h was placed directly after the reservoir. Three valves and a bypass allowed switching from an open to a closed system for respiration studies. A magnetic flow meter (Badger Meter, Isitec, Bremerhaven, Germany) was placed outside and in parallel to the Perspex tube to determine flow. Flow velocities were calibrated against an ultrasonic flow meter.

A round Perspex chamber closed on both sides with nylon grids contained the individual fish (maximum size of 50 cm body length and 1.2 kg body weight). It was connected to Kevlar threads at both ends and placed into the handling chamber (Fig. 1). The Kevlar threads were used to pull the chamber into the correct position in the center of the MR scanner. An integrated Perspex holder inside the chamber was used to fix the watertight surface coil relative to the tail muscle of the free moving fish and in parallel to the inductive coil [see Figs. 2(D,E)]. Velcro strips were used for fixation allowing easy repositioning and removal of the coil.

The temperature sensor, oxygen optodes, and cable of the water-sealed surface coil were fed through a seal in the handling chamber and connected to their specific instruments. The complete system except for the Perspex section inside the scanner was isolated with Arma Flex (Armacell International GmbH, Münster, Germany).

An underwater camera surrounded by a ring of blue LEDs was placed directly behind the animal chamber inside the Perspex tube for video observation of the swimming fish (Isitec, Bremerhaven, Germany). The camera holder and thus focus was adjustable relative to the animal chamber from outside via a plastic rod. The camera system was connected via a frame grabber to a PC equipped with video tracking software (MeDea AV, Erlangen, Germany). Analysis of differential pressure recordings as well as video sequences from the swimming behavior at different swimming speeds allowed the determination of tail beat frequencies and the onset of “kick and glide” bursts at critical swimming speeds.

All exercise studies were carried out with North Sea and North Eastern Arctic cod at 4 or 10°C, respectively. Both coil and fish blocking effects were calculated as described by Nelson et al. (20).

## Oxygen Consumption Measurements

An optical fiber system (“oxygen optodes”, Fibox, Presens, Germany) was used inside the MR system for oxygen consumption measurements. Briefly, a 5-m long optical fiber was fed into the animal handling chamber via a watertight seal and placed in the current of the swim tunnel. An oxygen-sensitive dye at the fiber’s tip detected changes in water oxygen concentrations. Optodes were calibrated at 0% air saturation with sodium dithionite and at 100% with air-saturated sea water. Temperature compensation of recordings was carried out manually. For oxygen consumption measurements, the complete sea water set-up system without an animal inside was tested by closure with the two valves in front of the reservoir.

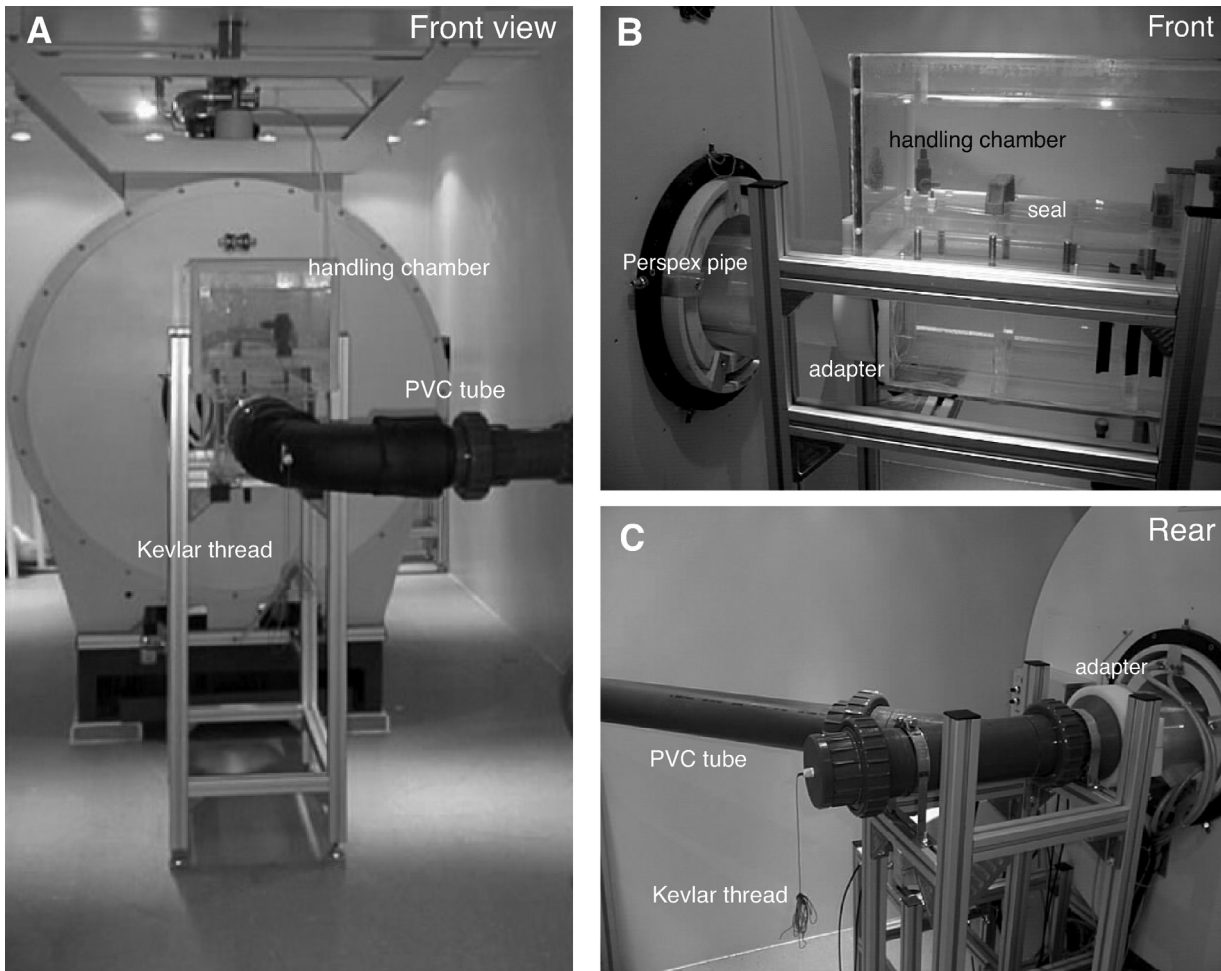


**Figure 1** (A) Photographic view of the swim tunnel feeding through the MRI scanner, with (B) front and (C) rear view, showing the Perspex pipe with the handling chamber prior the insulation with Armaflex. [Color figure can be viewed in the online issue, which is available at [www.interscience.wiley.com](http://www.interscience.wiley.com).]

Any decrease in water oxygen concentration during swimming performance of the animals could then be attributed to the oxygen consumption of the animal. Usually, the system was reopened and flushed after at about 30 min of swimming or a decrease by less than 20% of water air saturation during exercise to prevent any possible oxygen deprivation effects. The calibration of the system was repeated daily, to account for possible effects of bacterial respiration. The complete water volume was exchanged after each swimming trial.

### NMR Hardware

The negative effects of highly conductive sea water in a swim tunnel could only be marginally reduced,

as the animals could not be restrained. The sea water volume around the animals could only be limited to a certain degree in a way that swimming performance of the animal was not affected. The main contribution of a conducting sample like sea water is the inductive loss from eddy currents induced by the oscillating field  $B_1$ . The signal-to-noise ratio ( $S/N$ ) is basically proportional to the negative square root of the conductivity of the sample (15). The pulse length is also depending on the inductive losses resulting in a prolongation of the pulse or the need of higher power levels with increasing conductivity (15). Furthermore, the high dielectric permittivity increases the self-capacitance of the probe resulting in substantial changes of the matching and tuning properties. Our strategy for developing a usable NMR set-up there-

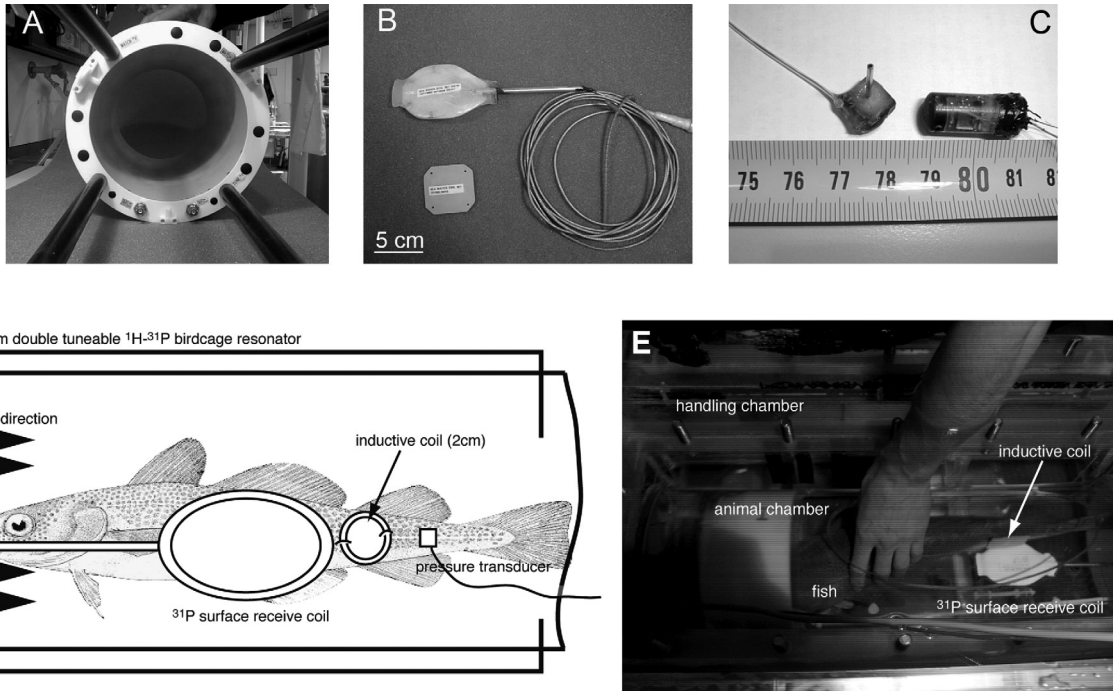


**Figure 2** (A) View through the 19.5 cm diameter seawater-adapted double tunable birdcage resonator used for the swim tunnel experiments. (B) Photograph of an inductive surface coil (left) and the watertight transmit/receive curved ellipsoid  $^{31}\text{P}$  surface coil before mounting (for more information see text). (C) Pressure transducer used for the gating experiments. (D) Schematic view of the experimental set-up illustrating all hardware components in combination. The arrows are indicating the flow direction. Figure 2(E) presents the in vivo situation at the beginning of the experiment. [Color figure can be viewed in the online issue, which is available at [www.interscience.wiley.com](http://www.interscience.wiley.com).]

fore relied mainly on the optimization of the specific NMR hardware. We basically divided the NMR excitation and perception signals in three parts:

1. A commercial double tunable  $^1\text{H}$ - $^{31}\text{P}$ -birdcage resonator [inner diameter 19.5 cm, Fig. 2(A)] adapted for very high loadings was used for signal excitation, specially developed and optimized for our purposes (Bruker-Biospin, Ettlingen, Germany). The inner Perspex tube of the swim tunnel fitted symmetrically inside the probe. The conductivity-induced changes of the matching and tuning properties were compensated with capacitors of broad capacitance range in the electrical circuit (property of Bruker), resulting in a reflection of less than 2% on both channels with a completely filled swim tunnel. Furthermore, both channels were optimized for a maximum RF-power of 2000 W to compensate for pulse length prolongations. The probe can be actively decoupled on both channels for use in cross-

coiled experiments in combination with surface coils to increase the  $S/N$  ratio. RF amplifiers used were a 2 kW  $^1\text{H}$ -amplifier operating at 200 MHz, and a 1 kW broadband amplifier for  $^{31}\text{P}$  NMR spectroscopy, respectively.

2. Inductive coils have the advantage that cable connections to the preamplifier can be avoided. Fixing the coil directly to the fish prevented further interference. Watertight 2 cm inner diameter inductive coils ( $^1\text{H}$  or  $^{31}\text{P}$ ) sealed in Teflon were developed for use in seawater [resulting size of around 4.5 cm length, see Fig. 2(B)]. Briefly, solenoid micro-coils were fabricated from copper and fixed tuned and matched on sea water and their specific resonance frequencies (200 and 81 MHz, respectively). Subsequently, the coil was placed in two Teflon plates and sealed. Small holes in each corner of the Teflon allowed the coil to be sutured to one side of the fish's tail. Exemplary, Fig. 2(B) presents a  $^{31}\text{P}$  inductive coil. The specific coil, for  $^1\text{H}$ - or  $^{31}\text{P}$  NMR,

respectively, was then sutured with two small sutures onto one side of the animal's tail with minimal effects on the swimming performance of the fish [see Figs. 2(D,E)].

3. A watertight transmit/receive curved ellipsoid  $^{31}\text{P}$  surface coil [inner diameters: 6 and 4 cm, respectively; outer diameter including plastic seal: 9 and 6 cm, Fig. 2(B)] developed for the swim tunnel application (Bruker-Biospin, Ettlingen, Germany) was placed onto the inner wall of the swim tunnel opposite the inductive coil. The coil was shaped to match the curvature of the fish, thereby improving excitation and reception [see Figs. 2(D,E)]. Match and tune capacitors of the coil were preset to the conductivity of seawater. Matching and tuning were individually optimized for the  $^{31}\text{P}$  channel using the active decoupling unit (Bruker, Ettlingen, Germany). The coil could be switched to a fixed matched and tuned  $^1\text{H}$  channel usable for shimming procedures only. One watertight cable was fed through a watertight adapter and connected to preamplifier and active decoupling unit of the MR scanner, respectively.

*In vivo*  $^{31}\text{P}$  NMR spectra were recorded during the swimming trails consecutively. Acquisition parameters were as follows: acquisition size 4 K, sweep width 5,000 Hz, flip angle  $45^\circ$ , bp32 pulse, pulse length 200  $\mu\text{s}$ , repetition delay 0.8 s, number of scans 256, resulting acquisition time 3.25 min. Despite of the short repetition time, no substantial relaxation effects could be observed similar to previous studies (21, 22) due to the fact that the  $T_1$  values of metabolites are greatly reduced in marine organisms. The repetition time was optimized comparing  $S/N$  ratio of  $^{31}\text{P}$  NMR spectra from a phosphate solution at different repetition times. Individual FIDs of every swimming speed were added for subsequent quantification of relative metabolite concentrations and the calculation of intracellular pH changes. Resulting spectra were processed using TopSpin 2.0 (Bruker, Ettlingen, Germany) with a zero filling of 8 K and a line broadening factor of 15 Hz. Peak position and signal integrals were analyzed using a specially adapted automatic fit routine as described in (21, 22). Metabolite concentrations from peak integrals were calculated as described in (23).

4. A separate set of experiments was performed with swimming cod equipped with a differen-

tial pressure transducer for better characterization of the swimming performance inside the MR integrated swim tunnel. Briefly, a differential pressure transducer [Fig. 2(C)] was fixed to the caudal fin of the fish and used to monitor tail beat pressures for the quantification of tail beat amplitude and frequency (for more information, see 17). Voltage thresholds set within the pressure pulses were used to gate MR measurements via a trigger box (Isitec, Bremerhaven, Germany), which was connected to the operator console of the MR imaging system and sending TTL pulses to the console via the EKG port of the spectrometer. The trigger pulse length and time before the onset of specific MR acquisition pulses could be defined such that MR spectra were sampled during tail beat pressure maxima, minima or pressure increments and decrements, respectively. The triggering allowed the gated acquisition of NMR spectra during maximum tail beat amplitude and minimum when the tail returned to his start position. The trigger box was connected to a PowerLab system (AD Instruments, Australia) for online monitoring of the pressure pulse and the correct setting of the trigger pulse. The trigger box was equipped with additional digital filters and a baseline compensation for the correction and smoothing of the tail beat pressure recordings.

## RESULTS AND DISCUSSION

The aim of this work was the development of a swim tunnel system integrated into a conventional MRI scanner for exercise studies in fish including analyses of oxygen consumption, work load, and muscle energy metabolism. Preliminary results of this work were presented by Pörtner et al. (18). A photographic view of the complete experimental set-up integrated to the magnet is shown in Figs. 1(A–C). Figure 2 presents the resonator [Fig. 2(A)], the surface coils [Fig. 2(B)], and the pressure transducer [Fig. 2(C)] used for the NMR studies to give an impression of the physical dimensions. A schematic depiction of the three different RF parts relative to each other together with the pressure transducer at the tail end of the fish is shown in Fig. 2(D). After surgery, the animal was placed into the chamber inside the animal handling chamber [Fig. 2(E)] and left there overnight for recovery at low flow, i.e. 1–2.5  $\text{m}^3/\text{h}$ . During this time, the fish usually started to swim freely against

the current inside the animal chamber. No movement restrictions were visible during this initial period of swimming for any fish. After recovery and confirmation of the right orientation of the coils relative to the fish and to each other, the animal chamber was pulled into the center of the magnet using the Kevlar threads. The exact positioning of animal chamber and coils relative to the resonator was confirmed by the camera system. Furthermore, standard gradient echo pilot scans in all three directions were performed prior to each swimming trial.

The animal handling chamber was closed and the resonator as well as the surface coil were matched and tuned. An automatic shimming routine (Bruker, Ettlingen, Germany) was used to provide field homogeneity. Indeed, since the swim tunnel resembled an ideal water-filled cylinder, line widths of 10 Hz of the water signal were reached easily as already described by Bock et al. (21, 22).

All parts of the NMR set-up were tested and optimized prior to exercise studies using a square bottle filled with 0.8 M  $\text{NaHPO}_3^-$  as a phantom. Figure 3 presents  $^{31}\text{P}$  NMR spectra from the phantom under different coil set-ups and positions of the sample relative to the surface receiver coil. Sagittal MR images over the entire animal chamber were obtained with a classical gradient echo sequence to locate the test set-up. Despite of the apparent magnetic field inhomogeneity over the entire field of view, position of phantom and coils could be determined in the images (Fig. 3, left). Interestingly, water flow had no influence on spectroscopic data, whereas blurring made it nearly impossible to get any information from MR images (data not shown). Therefore, water current was set to zero during imaging.

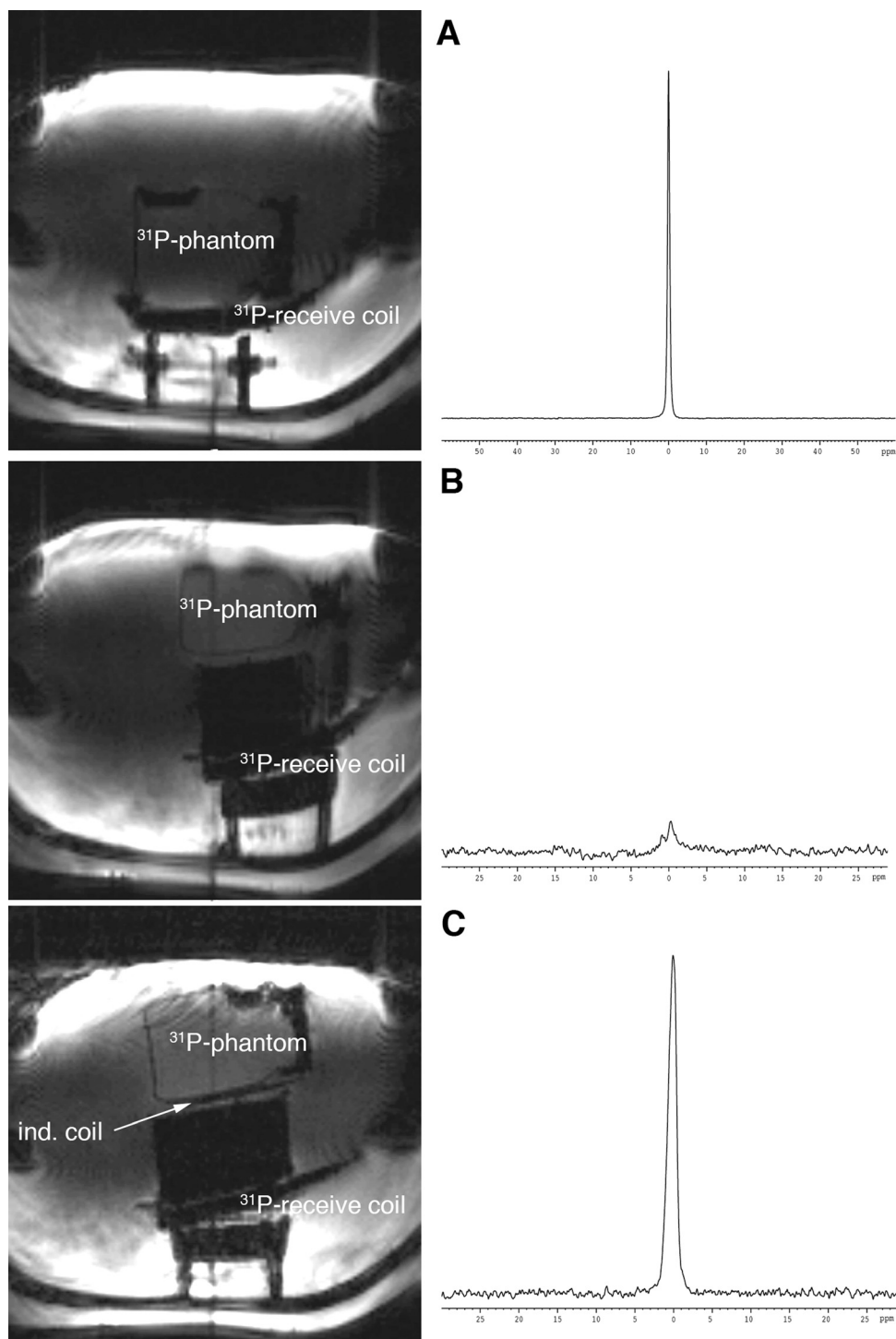
No signal could be detected using the resonator alone for  $^{31}\text{P}$  NMR spectroscopy (data not shown). This result is in line with the excitation profiles we observed using a standard gradient echo sequence (e.g., see bright contrast at the margin of the MR images, Fig. 3). Transverse MR images through the swim tunnel acquired with the birdcage resonator showed a very inhomogeneous excitation profile with highlighted areas near the edge of the swim tunnel indicating a strong skin effect. The skin effect also accounts for the signal loss when using the resonator for spectroscopy only. The RF excitation pulse from the resonator is reduced on its way through the seawater, such that the phantom could not be excited at all within the full power range of 2 kW of the RF amplifier (data not shown). Indeed, only the combination of resonator and elliptic surface receiver coil, operating in cross-coil operation mode, resulted in  $^{31}\text{P}$  NMR spectra with a sufficient signal-to-noise ra-

tio ( $S/N = 100$ ) after 128 acquisition pulses [resulting scan time 1.45 min, Fig. 3(A)]. Since the fish has to swim unrestricted with enough clearance to perform reliable exercise studies, the phantom was positioned 5 cm away from the receiver coil [Fig. 3(B)]. Placing a block between phantom and coil caused the  $^{31}\text{P}$  NMR signal to almost vanish resulting again in a fairly bad  $S/N$  ratio [see spectrum in Fig. 3(B)]. Nevertheless, addition of the inductive coil onto the phantom increased the  $S/N$  ratio to suitable values [around 30–40; Fig. 3(C)].

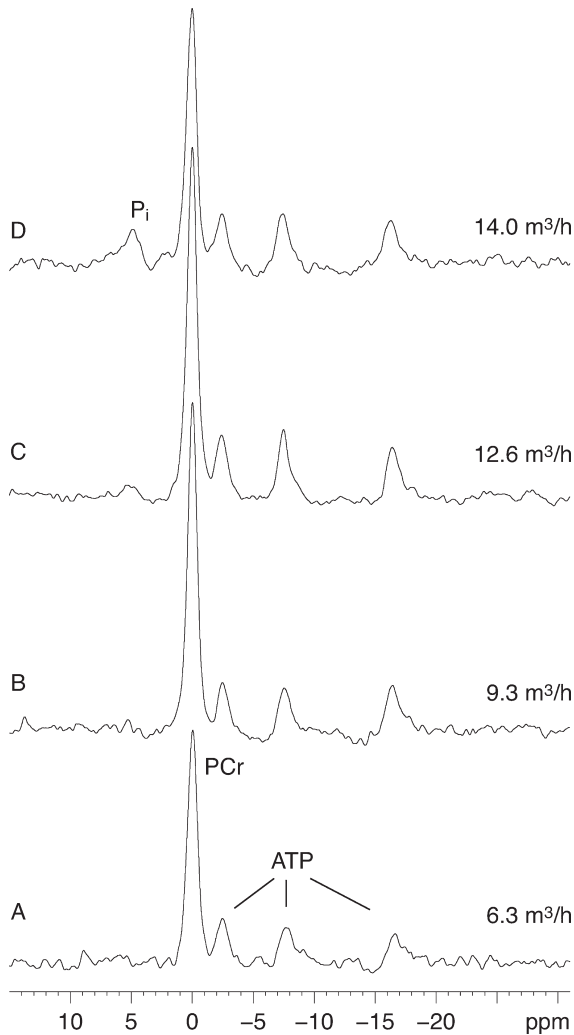
These results clearly demonstrate that only the combination of all three coils yielded sufficient  $S/N$  ratios on reasonable time scales and giving the animals enough free space for the exercise trials. Eddy currents and skin effect decrease RF power to an extent that the complete signal is almost lost on its way through the seawater. Nevertheless, the distance between inductive and receiver coils was suitable to prevent signal loss and helped to transport the RF signal through the seawater and on its way back. Overall, an increase in  $S/N$  ratio by about one order of magnitude could be reached with the three coil set-up in comparison to just using the  $^{31}\text{P}$  surface receive coil.

Figure 4(A) depicts typical *in vivo*  $^{31}\text{P}$  NMR spectra from swimming cod at different water currents. The presented spectra are the results of 9–13 individual spectra (of 256 scans resulting in 3.25 min) accumulated over the entire swimming trial (normally around 30 min) and depending on the oxygen consumption of the animals. At high swimming speeds, a decrease of around 20% of water air saturation could be observed already, resulting in shorter swimming periods for the animals (see Materials and Methods section). All spectra display clearly the most prominent phosphorus signals from muscle tissue, namely phosphocreatine (PCr) and the three signals of adenosine triphosphate (ATP) [Fig. 4(A)].

Interestingly, the line width of the signals in individual spectra decreased and the  $S/N$  ratio increased with increasing swimming speed despite the faster movement of the fish relative to the coil [Figs. 4(A,C), e.g. comparison of spectra at 12.6 and 6.3  $\text{m}^3/\text{h}$ , respectively]. At very low swimming speeds, animals moved back and forth in the tube and thus regularly changed position of the inductive relative to the receiver coil. At swimming speeds from 0.4 up to 1.2 body length/s (corresponding to flow rates of around 7 to a maximum of 14.0  $\text{m}^3/\text{h}$ ) depending on the size of the fish, the animal kept its position more or less stable during swimming, resulting in an equally stable position of the inductive relative to the receiver coil. Not until critical swimming speeds



**Figure 3** Comparison of  $^{31}\text{P}$  NMR spectra from a  $^{31}\text{P}$ -phantom solution placed into the center of the swim tunnel together with corresponding sagittal MR images of the set-up. (A)  $^{31}\text{P}$  NMR spectrum of the phantom positioned directly onto the surface coil (for acquisition parameters see text,  $S/N$  ratio = 100). (B)  $^{31}\text{P}$  NMR spectrum of the phantom placed at a distance of around 5 cm relative to the surface coil. Almost no signal could be detected from the phantom. (C)  $^{31}\text{P}$  NMR spectrum of the phantom at the same position with attached inductive coil (the arrow indicates the location of the coil in the sagittal view,  $S/N$  = 35).



**Figure 4** Accumulated in vivo  $^{31}\text{P}$  NMR spectra from Atlantic cod at different swimming speeds. Figure 4(A) presents a  $^{31}\text{P}$  NMR spectrum at a flow of  $6.3\text{ m}^3/\text{h}$  corresponding to a swimming speed of 0.2 body length/s. Phosphocreatine (PCr) and the three ATP signals can be clearly resolved (for acquisition parameters see text, line broadening 30 Hz). (B,C) In vivo  $^{31}\text{P}$  NMR spectra from the tail muscle of swimming cod at moderate swimming speeds ( $9.3$  and  $12.6\text{ m}^3/\text{h}$ , respectively), resulting in no obvious differences to spectra at slower swimming speeds, despite a higher  $S/N$  ratio. Figure 4(D) shows the energetic situation at critical swimming speed, when cod started to use kick and glide swimming ( $14\text{ m}^3/\text{h}$ , around 1.0 body length/s). Note the decrease in PCr accompanied by the onset of inorganic phosphate (Pi) accumulation.

were reached, the quality of the spectra decreased again. In Fig. 4(D), for instance, an in vivo  $^{31}\text{P}$  NMR spectrum of the same animal swimming near the critical swimming speed is presented ( $14\text{ m}^3/\text{h}$ , 1.0 body length/s). The critical swimming speed has recently

been defined as the point, when the fish started using “kick and glide” bursts and exploited high energy phosphates while maintaining position in the swim tunnel (16, 18). “Kick and glide” bursts are typically used during escape swimming or hunting prey and are powered by anaerobic white muscle, whereas “normal” subcarangiform swimming employs red aerobic muscle. Using white musculature for faster swimming is fuelled by anaerobic metabolism and therefore time limited. The metabolic situation during swimming bursts and the use of anaerobic white muscle is clearly reflected in the spectrum displayed in Fig. 4(D). PCr decreased in comparison to moderate swimming and the accumulation of inorganic phosphate (Pi, see spectrum 4D) is detected. Furthermore, intracellular pH, derived from the position of the inorganic phosphate signal, decreased. A drop in intracellular muscle pH values during exercise despite the alkalizing effect of phosphocreatine depletion gives strong evidence for lactate production (24) and is therefore indicative of limited aerobic energy supply and the onset of anaerobic metabolism. A brief quantitative analysis of in vivo  $^{31}\text{P}$  NMR data from four individuals is presented in Fig. 5. The graph displays concentration changes of the high-energy phosphates [PCr, ATP, and inorganic phosphate (Pi)] from muscle tissue at increasing swimming speeds. Swimming speeds are expressed as mean water flow in  $\text{m}^3/\text{h}$ . A significant increase of inorganic phosphate could be observed at swimming speeds around  $13\text{ m}^3/\text{h}$ , confirming the use of white musculature, the onset of anaerobic metabolism, and the reaching of critical swimming speed. No significant changes in PCr and ATP levels could be

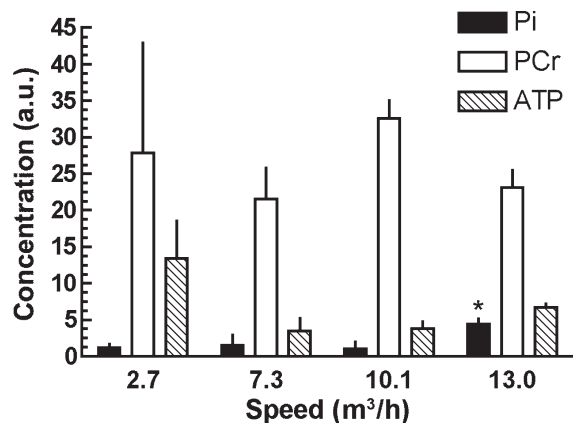


**Figure 5** In vivo  $^{31}\text{P}$  NMR metabolite concentration changes of fish tail muscle at different swimming speeds ( $n = 4$ ). At a mean swimming speed of  $13\text{ m}^3/\text{h}$ , a significant increase of inorganic phosphate could be observed indicating the onset of anaerobic metabolism.

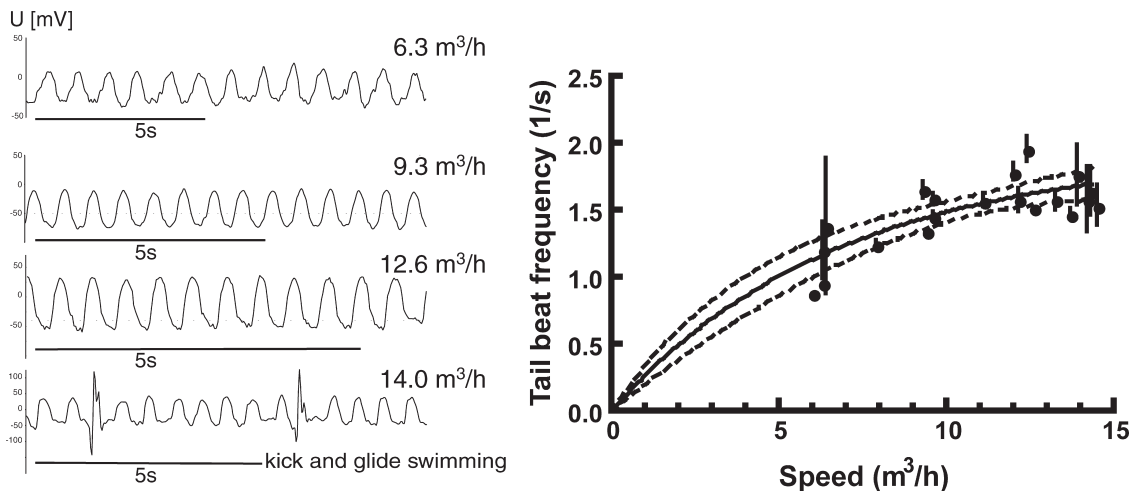


**Figure 6** Left: Individual pressure traces from same individual as in Fig. 4 at different swimming speeds. Note the spikes in the trace at 14 m<sup>3</sup>/h mark the onset of “kick and glide” swimming. Right: Mean tail beat frequency is presented in relation to swimming speed ( $n = 4$ ). Tail beat frequency increased with swimming speed until the critical swimming speed was reached. Maximum values are indicating the onset of kick and glide swimming near the critical swimming speed. The point when critical swimming speed is reached fits perfectly with the onset of intracellular acidification and the onset of inorganic phosphate accumulation as shown in Figs. 4 and 5 (see also 16, 18).

observed, most likely due to high individual variability. Indeed, in our accompanying paper presenting a more complete and time-resolved analysis of the bioenergetics; the observed increase in Pi was coupled with a stoichiometric decrease in the relative proportion of PCr, whereas free ATP did not change significantly during the swimming trials. Intracellular pH decreased from around pH 7.48 to a minimal pH of 6.81 at critical swimming speeds indicating lactate formation (16).

Results from the initial set of experiments using NMR spectroscopy together with the differential pressure transducer are presented in Fig. 6. On the left part of the figure, typical pressure recordings from increasing swimming speeds are presented. The smooth sine curve of the traces is reflecting the tail movement and indicates controlled swimming. The spikes in the trace of the highest swimming speed resulted from the additional “kick and glide” swimming trials. On the right part of the figure, the results from the pressure traces are summarized. Mean tail beat frequency increased with swimming speed and leveled off when critical swimming speed was reached. Maximum critical swimming speed was around 70% of that compared to literature values from swimming cod (17, 20, 25, 26), but are in line with observations from experiments on similar sized

cod using pressure transducers (Gamperl, personal communication). Additionally, the recordings obtained with the pressure transducer allowed us to set trigger values for the acquisition of <sup>31</sup>P NMR spectra. In this way, spectra could be recorded at specific tail and therefore inductive coil positions relative to the receiver coil resulting in improved S/N ratios together with narrower line widths of the signals. Figure 7 shows an example of three gated *in vivo* <sup>31</sup>P NMR spectra at a flow rate of 9.3 m<sup>3</sup>/h. The lower spectrum was triggered on the maxima of the pressure trace; the middle spectrum was triggered at the rising edge and the upper spectrum was gated on the minima of the pressure trace. The various trigger settings resulted in substantial differences of the S/N ratio with the best quality showing the spectrum gated on the minima. This trigger set point reflected the optimal position of inductive coil in relation to the receive coil resulting in the highest S/N ratio. Gating is especially advantageous at higher swimming speeds, i.e. near the critical swimming speed when animals started to use “kick and glide” bursts (see spikes in pressure trace at 14.0 m<sup>3</sup>/h of Fig. 6). Furthermore, triggering allows acquisition of time-resolved <sup>31</sup>P NMR spectra for analyzing the metabolic machinery during exercise as for instance previously has been carried out in squid (27).

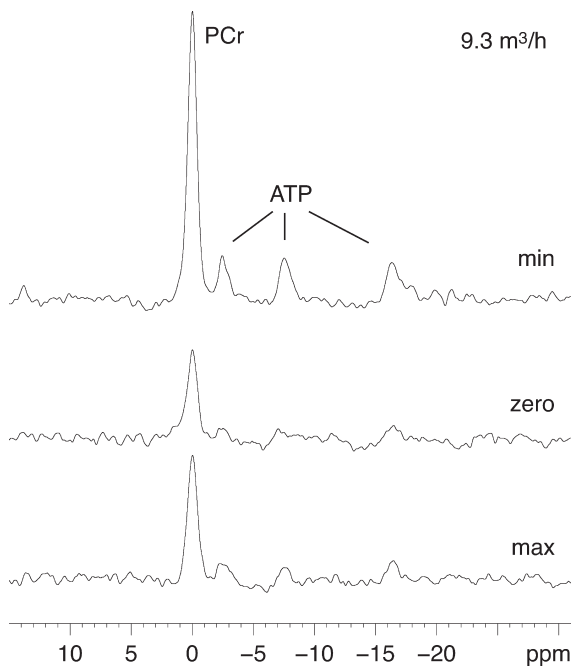


**Figure 7** Example of three gated in vivo  $^{31}\text{P}$  NMR spectra at a flow rate of  $9.3 \text{ m}^3/\text{h}$  and different trigger settings according to the pressure trace from Fig. 6. Note the different  $S/N$  ratios obtained with different trigger set points.

## CONCLUSIONS AND PERSPECTIVES

This paper describes an integrated swim tunnel set-up for online in vivo  $^{31}\text{P}$  NMR spectroscopy studies of exercising marine fish.  $^{31}\text{P}$  spectra were accumulated at sufficient  $S/N$  ratios within minutes allowing the characterization of energy metabolism and acid base regulation of working tail muscle (see 16, 18) in combination with oxygen consumption measurements (data not shown). Using differential pressure transducers improved spectra quality and allowed to trigger and monitor spectra during specific contraction phases and the resulting metabolic situation (18, 27). As the use of differential pressure transducers is invasive, a next step will use the integrated camera system combined with online video analysis software for noninvasive triggering and online determination of swimming performance.

## ACKNOWLEDGMENTS

This work was made possible by an equipment grant of the Federal Minister for Education and Research to the AWI (H.O. Pörtner). We like to thank our scientific workshop at the AWI for construction of the MR integrated swim tunnel. The

support by Dr. Sven Junge and his group from Bruker-Biospin MRI during development and construction of the sea water-adapted RF-coils is highly appreciated.

## REFERENCES

1. Pörtner HO. 2002. Physiological basis of temperature-dependant biogeography: trade-offs in muscle design and performance in polar ectotherms. *J Exp Biol* 205:2217–2230.
2. Pörtner HO. 2002. Environmental and functional limits to muscular exercise and body size in marine invertebrate athletes. *Comp Biochem Physiol A Mol Integr Physiol* 133:303–321.
3. Pörtner HO, Lucassen M, Storch D. 2005. Metabolic biochemistry: its role in thermal tolerance and in the capacities of physiological and ecological function. In: Farrell AP, Steffensen JF, eds. *The Physiology of Polar Fishes*. San Diego, CA: Elsevier Academic Press. pp 79–154.
4. Davidson W. 2005. Antarctic fish skeletal muscle and locomotion. In: Farrell AP, Steffensen JF, eds. *The Physiology of Polar Fishes*. San Diego, CA: Elsevier Academic Press. pp 317–350.
5. DeVries AL, Cheng CHC. 2005. Antifreeze proteins and organismal freezing avoidance in polar fishes. In: Farrell AP, Steffensen JF, eds. *The Physiology of Polar Fishes*. San Diego, CA: Elsevier Academic Press. pp 155–202.
6. Storelli C, Acierno R, Maffia M. 1998. Membrane lipid and protein adaptations in Antarctic fish. In: Pörtner HO, Playle R, eds. *Cold Ocean Physiology*. Society for Experimental Biology Seminar Series. Cambridge: Cambridge University Press. pp 166–189.
7. Desaulniers N, Moerland TS, Sidell BD. 1996. High lipid content enhances the rate of oxygen diffusion through fish skeletal muscle. *Am J Physiol Regul Integr Comp Physiol* 271:R42–R47.
8. Johnston IA. 1982. Capillarisation, oxygen diffusion distances and mitochondrial content of carp muscles following acclimation to summer and winter temperatures. *Cell Tissue Res* 222:325–337.
9. Hardewig I, Van Dijk PLM, Pörtner HO. 1998. High-energy turnover at low temperatures: recovery from exhaustive exercise in Antarctic and temperate eelpouts. *Am J Physiol Regul Integr Comp Physiol* 274: R1789–R1796.
10. Pörtner HO, Knust R. 2007. Climate change affects marine fishes through the oxygen limitation of thermal tolerance. *Science* 315:95–97.
11. Brett JR. 1967. Swimming performance of sockeye salmon (*Oncorhynchus nerka*) in relation to fatigue time and temperature. *J Fish Board Canada* 24:1731–1741.
12. Steffensen JF. 2005. Respiratory systems and metabolic rates. In: Farrell AP, Steffensen JF, eds. *The Physiology of Polar Fishes*. San Diego, CA: Elsevier Academic Press. pp 203–238.

13. Farrell AP, Clutterham SM. 2003. On-line venous oxygen tensions in rainbow trout during graded exercise at two acclimation temperatures. *J Exp Biol* 206:487–496.
14. Burgetz IJ, Rojas-Vargas A, Hinch SG, Randall DJ. 1998. Initial recruitment of anaerobic metabolism during sub-maximal swimming in rainbow trout (*Oncorhynchus*). *J Exp Biol* 201:2711–2721.
15. Kugel H. 1991. Improving the signal-to-noise ratio of NMR signals by reduction of inductive losses. *J Magn Reson* 91:179–185.
16. Lurman GJ, Bock C, Pörtner HO. 2007. An examination of the metabolic processes under-pinning critical swimming in Atlantic cod (*Gadus morhua* L.) using in vivo  $^{31}\text{P}$ -NMR spectroscopy. *J Exp Biol* 210:3749–3756.
17. Webber DM, Boutilier RG, Kerr SR, Smale MJ. 2001. Caudal differential pressure as a predictor of swimming speed of cod (*Gadus Morhua*). *J Exp Biol* 204:3561–3570.
18. Pörtner HO, Webber DM, Bock C, Wittig RM. 2002. In vivo  $^{31}\text{P}$ -NMR studies of speeding fish: online monitoring of muscular energetics in Atlantic cod (*Gadus morhua*). *Proc Intl Soc Magn Reson Med* 10: 1878.
19. Bock C, Pörtner HO, Wittig RM, Webber DM, Junge S. 2002. An insulated three coil set-up for MR studies on swimming fish operating in sea water. *Proc Intl Soc Magn Reson Med* 10:871.
20. Nelson JA, Tang Y, Boutilier RG. 1994. Differences in exercise physiology between two Atlantic cod (*Gadus morhua*) populations from different environments. *Physiol Zool* 67:330–354.
21. Bock C, Wittig RM, Sartoris FJ, Pörtner HO. 2001. Temperature dependent pH regulation in stenothermal Antarctic and eurythermal temperate eelpout (*Zoarcididae*): an in vivo NMR study. *Polar Biol* 24:869–874.
22. Bock C, Sartoris FJ, Pörtner HO. 2002. In vivo MR spectroscopy and MR imaging on non-anaesthetized marine fish: techniques and first results. *Magn Reson Imaging* 20:165–172.
23. Sartoris FJ, Bock C, Serendero I, Lannig G, Pörtner HO. 2003. Temperature dependent changes in energy metabolism, intracellular pH and blood oxygen tension in the Atlantic cod, *Gadus morhua*, *Journal Fish Biol*, 62:1239–1253.
24. Pörtner HO. 1987. Contributions of anaerobic metabolism to pH regulation in animal tissues: theory. *J Exp Biol* 131:69–87.
25. Reidy SP, Kerr SR, Nelson JA. 2000. Aerobic and anaerobic swimming performance of individual Atlantic cod. *J Exp Biol* 203:347–357.
26. Reidy SP, Nelson JA, Tang Y, Kerr SR. 1995. Post-exercise metabolic rate in Atlantic cod and its dependence upon the method of exhaustion. *J Fish Biol* 47:377–386.
27. Pörtner HO, Lee PG, Webber DW, O'Dor RK, Bock C, Quast M. 1998. Studying the metabolic machinery of contracting squid mantle muscle in vivo: a time resolved  $^{31}\text{P}$ -NMR study. *Proc Intl Soc Mag Reson Med* 6:1803.

Author Proof